configurations. It is shown that these filters are valuable for real-time image and video coding and are very easy to implement on VLSI.

It should be emphasized that the codec structures implemented here did not have any visually justified fine tuning, Q-tables, etc., in bit allocation or in quantization steps, in order to obtain an unbiased performance comparison of different filter banks and block transforms. Therefore, the image coding performance presented in this correspondence is not competitive with the state-of-the-art solutions available in the literature. This tuning step is a topic of future study.

VI. Conclusions

It is shown in this correspondence that two-band multiplierless suboptimal PR-QMF solutions exist. Their objective and subjective performance in subband image coding are comparable or better than known subband- and DCT-based codecs for the scenarios considered. The multiplierless PR-QMF's are expected to be used in real-time image and video processing and coding.

Acknowledgment

Some of the simulations presented in Section V were performed during the author's visit to GEC-Marconi Electronic Systems Inc., Totowa, NJ, in 1992. The author would like to thank R. Buell and D. Cooper of GEC-Marconi for their valuable discussions and for providing him with the image prints.

References

[1] H. S. Malvar, "The LOT: a link between transform coding and multirate filter banks," in *Proc. Int. Symp. Circuits Syst.,* 1988, pp. 835–838.
[2] A. N. Akansu and R. A. Haddad, *Multiresolution Signal Decomposition: Transforms, Subbands and Wavelets.* New York: Academic, 1992.
[3] M. Smith and T. P. Barnwell, "Exact reconstruction techniques for tree structure subband coders," *IEEE Trans. Acoust., Speech, Signal Processing,* pp. 434–441, 1986.
[4] F. Mintzer, "Filters for distortion-free two-band multirate filter banks, *IEEE Trans. Acoust., Speech, Signal Processing,* vol. 33, pp. 626–630, June 1985.
[5] P. P. Vaidyanathan, "Quadrature mirror filter banks, M-band extensions and perfect reconstruction techniques," *IEEE Acoust., Speech, Signal Processing,* pp. 4–20, July 1987.
[6] M. Vetterli and D. LeGall, "Perfect reconstruction FIR filter banks: some properties and factorizations," *IEEE Trans. Acoust., Speech, Signal Processing,* pp. 1051–1071, July 1989.
[7] H. S. Malvar and D. H. Staelin, "The LOT: transform coding without blocking effects," *IEEE Trans. Acoust., Speech, Signal Processing,* vol. 37, pp. 553–559, Apr. 1989.
[8] "Video compression, new standards, new chips," *IEEE Spectrum,* Oct. 1991.
[9] H. Gharavi and A. Tabatabai, "Subband coding of digital image using two-dimensional quadrature mirror filtering," in *Proc. SPIE Visual Commun. Image Processing,* 1986, pp. 51–61.
[10] J. W. Woods, S. D. O'Neil, "Subband coding of images," *IEEE Trans. Acoust., Speech, Signal Processing,* vol. ASSP-34, no. 5, Oct. 1986.
[11] A. N. Akansu, and Y. Liu, "On signal decomposition techniques," *Opt. Eng.,* pp. 912–920, July 1991.
[12] I. Daubechies, "Orthonormal bases of compactly supported wavelets," *Commun. Pure Appl. Math.,* vol. XLI, pp. 909–996, 1988.
[13] H, Caglar, Y. Liu, and A. N. Akansu, "Statistically optimized PR-QMF design," in *Proc. SPIE Visual Commun. Image Processing,* Nov. 1991, pp. 86–94.
[14] R. A. Haddad, A. N. Akansu and A. Benyassine, "Time-frequency localization in transforms, subbands and wavelets: a critical review," *Opt. Eng.,* pp. 1411–1429, July 1993.
[15] N. S. Jayant, and P. Noll, *Digital Coding of Waveforms.* Englewood Cliffs, NJ: Prentice-Hall, 1984.
[16] A. N. Akansu, R. A. Haddad, and H. Caglar, "The binomial QMF-wavelet transform for multiresolution signal decomposition," *IEEE Trans. Signal Processing,* vol. 41, pp. 13–19, Jan. 1993.
[17] I. Daubechies, "Orthonormal bases of compactly supported wavelets II: variations on a theme," AT&T Bell Labs, Murray Hill, NJ, Tech. Memo 11217-891116-17, and private communication.
[18] J. W. Woods and T. Naveen, "A filter-based bit allocation scheme for subband compression of HDTV," *IEEE Trans. Image Processing,* vol. 1, pp. 436–440, July 1992.
[19] A. N. Akansu, "Multiplierless 2-band perfect reconstruction quadrature mirror filter (PR-QMF) banks," U.S. Patent 5,420,891, May 30, 1995.

Artifact Reduction in Low Bit Rate DCT-Based Image Compression

Jiebo Luo, Chang Wen Chen, Kevin J. Parker, and Thomas S. Huang

***Abstract*—This correspondence presents a scheme for artifact reduction of low bit rate discrete-cosine-transform-compressed (DCT-compressed) images. First, the DC coefficients are calibrated using gradient continuity constraints. Then, an improved Huber–Markov-random-field-based (HMRF-based) smoothing is applied. The constrained optimization is implemented by the iterative conditional mode (ICM). Final reconstructions of typical images with improvements in both visual quality and peak signal-to-noise ratio (PSNR) are also shown.**

I. Introduction

Discrete-cosine-transform-based (DCT-based) compression has been the most popular among many existing image compression techniques. The DCT has very good energy compaction and decorrelation properties. Moreover, the DCT can be computed using fast algorithms and efficiently implemented using very large scale integration (VLSI) techniques. In DCT-based coding, an image is partitioned into small square blocks (typically 8×8) and the DCT is computed over these blocks to remove the local spatial correlation. In order to achieve high compression, quantization of the DCT coefficients is then performed [1], [2]. Quantization is an irreversible process that causes loss of information and distortions in the decompressed image. After quantization, the redundancy of the data is further reduced using entropy coding. At the decoder end, the received data is decoded, dequantized, and reconstructed by the inverse DCT. In general, a typical 8-b gray-level image can be coded with compression ratios up to 10 : 1 without noticeable artifacts.

However, at low bit rates the reconstructed images generally suffer from visually annoying artifacts as a result of very coarse quantization. One major such artifact is the blocking effect, which appears as artificial block boundaries between adjacent blocks. At

Manuscript received May 31, 1994; revised October 18, 1995. This work was supported by NSF under Grant EEC-92-09615 and by a New York State Science and Technology Foundation Grant to the Center for Electronic Imaging Systems at the University of Rochester. The associate editor coordinating the review of this manuscript and approving it for publication was Prof. William A. Pearlman.

J. Luo, C. W. Chen, and K. J. Parker are with the Department of Electrical Engineering, University of Rochester, Rochester, NY 14627 USA (e-mail: luo@ee.rochester.edu).

T. S. Huang is with the Beckman Institute and Coordinated Science Laboratory, University of Illinois at Urbana-Champaign, Urbana, IL 61801 USA.

Publisher Item Identifier S 1057-7149(96)05252-9.

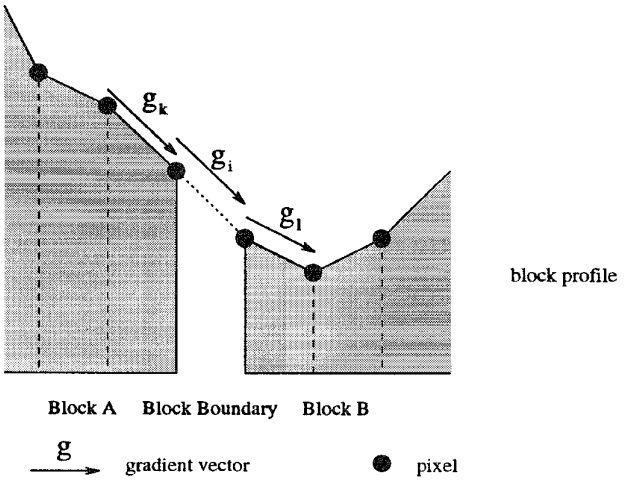

Fig. 1. Illustration of the gradient continuity constraint.

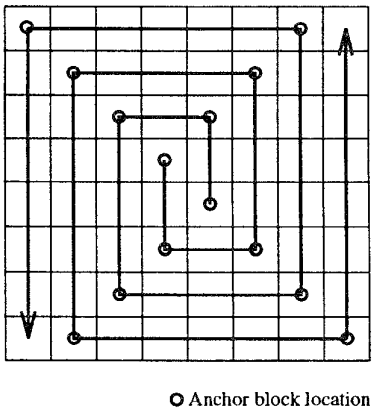

Fig. 2. Anchor blocks and the double spiral scan.

a low bit rate, each block is represented mainly by the first few low-frequency coefficients and, since each block is processed independently, no interblock correlation is accounted for in standard block DCT-based coding schemes. Therefore, discontinuity across the block boundary becomes noticeable. There are many techniques developed to reduce the blocking effect. Some increase the bit rate substantially or change the coding and decoding procedure dramatically [3], or even give rise to other artifacts such as the ringing effect [4]. In general, postprocessing at the decoder side only is very much desired because it causes the least change to the overall compression and transmission scheme. Postprocessing is generally implemented as image filtering—either linear filtering [3] or more sophisticated nonlinear filtering [5]. To preserve the edges, edge segments in the compressed image may be estimated before smoothing [5], [6]. However, it is very hard to accurately differentiate true edges from the artifacts at low bit rates. Some techniques formulate the blocking effect removal as image restoration problems [7], [8]. A Huber–Markov random field (HMRF) model was first introduced in [9] to form a maximum *a posteriori* (MAP) estimation of the decompressed image. Another type of artifact is the ringing effect, which is caused by the loss of high-frequency coefficients and appears as ringing patterns around sharp edges. The ringing effect is particularly prominent in images that are of high contrast and contain sharp edges and thin structures, such as document images. In order not to blur these images, edge-preserving nonlinear filtering is desired. However, there has been little investigation on this aspect until recently [10]. The ability to reduce both types of artifacts is especially valuable at low bit rates.

The DC coefficients are of particular importance at low bit rates, where many high-frequency coefficients are discarded and the coarse quantization of the DC coefficients generally causes the reference level of each block to vary within a relatively large quantization interval. Therefore, the calibration of the reference level of a block is very much desired before we apply viable smoothing techniques to the image. Otherwise, an improvement in image quality, especially in terms of PSNR, cannot be achieved, even though a visually pleasing image may be produced by smoothing the artificial block boundaries.

We propose a two-step approach to the artifact-reduction problem. First, a DC calibration is performed in a block-by-block fashion based on gradient continuity constraints over the block boundaries. Then, a modified Huber–Markov random field model is employed to formulate a convex constrained restoration problem. A similar technique has been shown able to smooth the artificial discontinuities [9] while preserving the remaining details of the original image. We make two very important modifications to this technique [9]. First, we designate two Huber–Markov random field models in order to differentiate the pixels on the block boundary from those inside the block. This allows the artifacts along the block boundaries to be smoothed and the details inside the block to be preserved. Second, and more important, we apply a different *local* optimization technique, the *iterative conditional mode* (ICM) [11], to implement the smoothing algorithms so that the *localized* spatial constraints can be accurately enforced.

Throughout the following sections, uppercase letters are used to denote random variables and lowercase letters for the corresponding realizations. A random field X will be defined on a set of sites S, i.e., a set of $N \times N$points. $X_s \in \mathcal{R}$ denotes a pixel at site s. Bold uppercase letters denote matrixes or transformations.

II. MAP Estimation

Bayesian estimation is a frequently employed approach to ill-posed inverse problems by incorporating the *a priori* probability of the random field X [12]. Maximum *a posteriori* (MAP) estimation has been very powerful given the observed data Y and a reasonable *a priori* distribution $p(X)$. A MAP-based estimation that maximizes the *a posteriori* probability can generally be written as

$$\hat{x} = \arg\max_{\boldsymbol{X}} p(x|y) \tag{1}$$

The optimization can be conveniently rewritten using the Bayes' rule and the log-likelihood function

$$\hat{x} = \arg\max_{\boldsymbol{X}} \{\log p(y|x) + \log p(x)\}. \tag{2}$$

In the case of restoring a decompressed image, $p(x)$ is the *a priori* probability of the two-dimensional (2-D) random field X and $p(y|x)$ represents the conditional probability of the compressed Y given the original image X.

A. Image Prior Model

Markov random fields have been utilized to model images in many image processing applications, and are adopted to model the *a priori* probability $p(x)$ in (2). As was proved by the Hammersley–Clifford Theorem [12], there exists an equivalence between a Markov random field and a Gibbs random field. A Gibbs random field is characterized by a Gibbs distribution, which provides a simple and practical way of parameterizing MRF's by potential functions, instead of the local

Fig. 3. Illustrations of artifacts reduction. Top left: original Lena image. Top right: standard decompression. Bottom left: ICM without DC calibration. Bottom right: ICM with DC calibration.

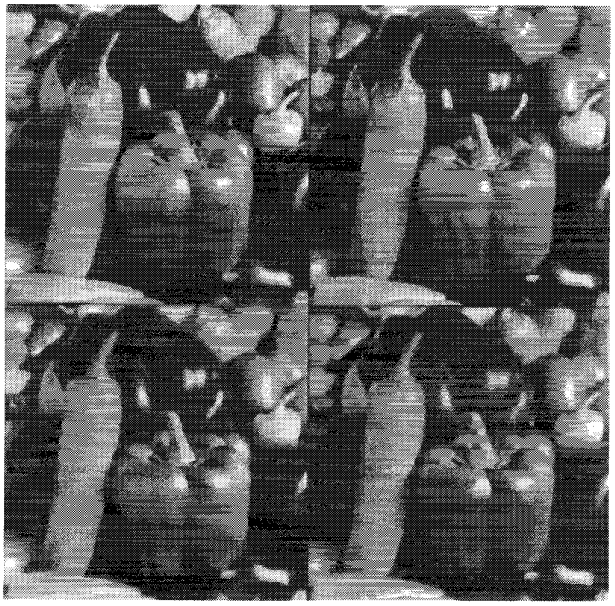

Fig. 4. Illustrations of artifacts reduction. Top left: original Peppers image. Top right: standard decompression. Bottom left: ICM without DC calibration. Bottom right: ICM with DC calibration.

characteristics of the random field. A general form of the Gibbs distribution can be written as

$$p(x) = \frac{1}{Z} \exp\left\{ -\sum_{c \in C} V_c(x) \right\} \tag{3}$$

where Z is a normalization constant and V_c is a certain clique potential function for clique c. Clique c is a local group of pixels, while C is the set of all such local groups. The neighborhood of a pixel at site s is denoted by $\partial s \subset S$ where S is the set of all sites. If c is defined such that $\forall s, r \in c, s$ and r are neighbors, then the clique has the property that

$$\forall s, r \in S, s \notin \partial s, r \in \partial s \Leftrightarrow s \in \partial r. \tag{4}$$

Moreover, the essential property of an MRF

$$\forall s \in S, p(x_s | x_r, \forall r \neq s) = p(x_s | x_r, r \in \partial s) \tag{5}$$

means that the conditional probability depends only on the neighborhood constraints. This property facilitates the ICM implementation described in Section IV.

Stevenson [9] has investigated a type of convex function known as the Huber minimax function, as follows:

$$\rho(\Delta) = \begin{cases} \Delta^2, & |\Delta| \leq T \\ T^2 + 2T|\Delta| - T|, & |\Delta| > T \end{cases} \tag{6}$$

as a suitable potential function for the Gibbs distribution. The quadratic segment of the function imposes least-mean-square smoothing to small discontinuities Δ of magnitude smaller than T. However, for Δ greater than T, the linear segment of the function imposes a much lighter penalty and preserves sharp transitions such as edges. Note that since this function belongs to $\boldsymbol{C}^1$, its first derivative is continuous so that unnatural results are unlikely to occur. An MRF characterized by a Huber function is an HMRF. The parameter T controls not only the threshold to switch between the quadratic segment and the linear segment, but also the slope of the linear segment. Therefore, it plays a crucial role in determining the behavior of the HMRF.

We modify the HMRF model to suit this particular application where we need to differentiate the true image edges from the artifacts. A single value of T is clearly inadequate to describe all the discontinuities, and in particular, is unable to differentiate true image edges from artifacts. Since the mechanism that generates the artifacts, and the locations of the blocking artifact, are known in DCT-based coding, we can incorporate such information to improve the HMRF model for this specific application. The discontinuities inside each image block are produced in a different way from those along the block boundaries. Inside the block, the distortions are caused by the quantization and the truncation of high frequency components. Along the block boundaries, further distortions are introduced because no correlation is exploited across the boundaries. The artificial block boundaries can be considered as some extra high frequency energy [7] and hence require additional smoothing. Therefore, these two types of discontinuities should be handled separately. In this research, a relatively larger parameter value of $T = T1$ is employed in the local HMRF model for those pixels in the boundary regions in order to smooth the artifacts, while a moderate value of $T = T2$ is applied to the inner block regions.

B. Image Compression Model

A class of lossy transform image coding can be modeled as

$$Y = \boldsymbol{Q}[\boldsymbol{H}(X)] \tag{7}$$

where X is the original image, $\boldsymbol{H}$ stands for certain transform, $\boldsymbol{Q}[\cdot]$ is a designated quantization operation (scalar or vector), and Y is the lossy image representation. In DCT-based coding, $\boldsymbol{H}$ is the DCT, $\boldsymbol{Q}[\cdot]$ is a scalar quantization, and Y consists of the quantized coefficients that generally need fewer bits to represent. Since $\boldsymbol{Q}[\cdot]$ is a noiseless many-to-one mapping, the conditional probability $P(Y|X)$ can be written as

$$P(Y|X) = \begin{cases} 1, & Y = \boldsymbol{Q}[\boldsymbol{H}(X)] \\ 0, & Y \neq \boldsymbol{Q}[\boldsymbol{H}(X)]. \end{cases} \tag{8}$$

Because the human visual system is relatively insensitive to high-frequency energy, zonal sampling is often adopted so that only

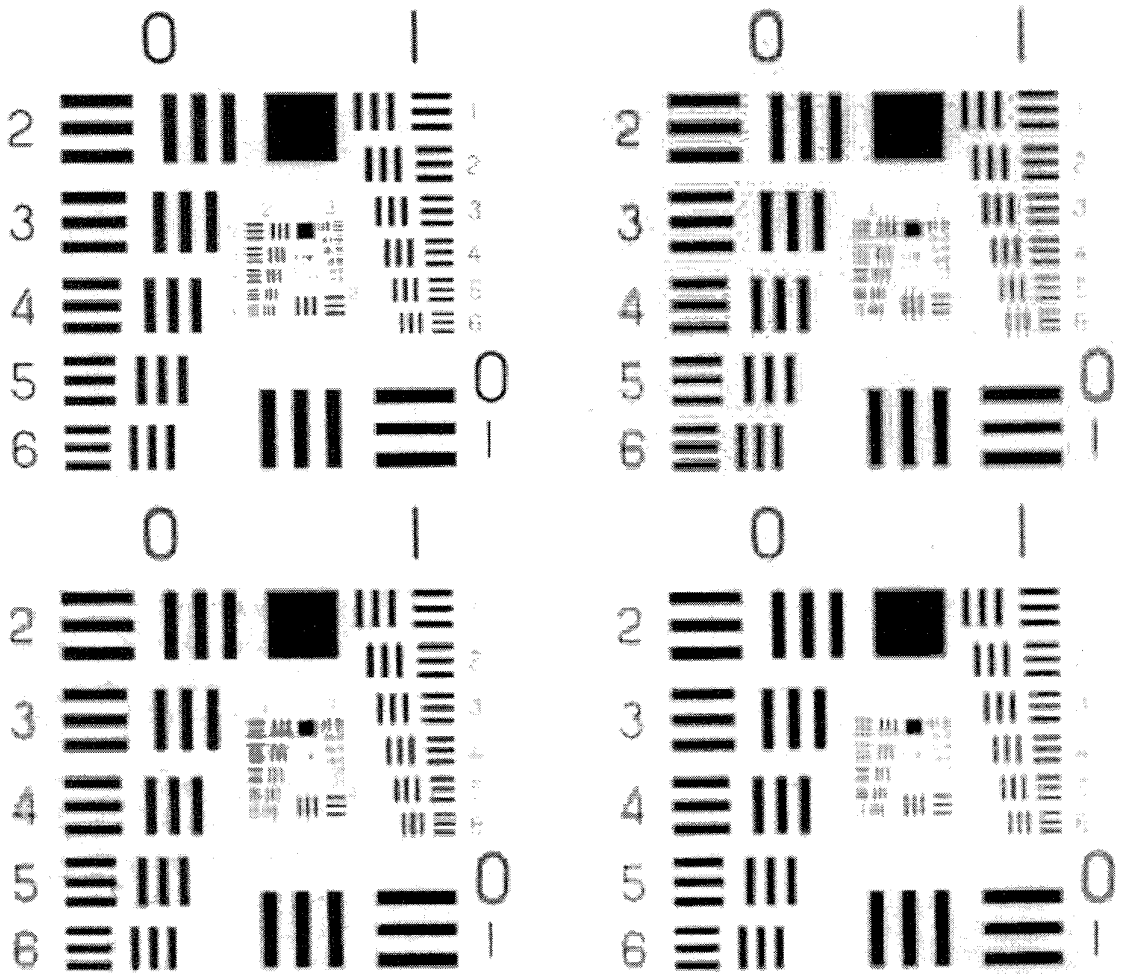

Fig. 5. Illustrations of artifacts reduction. Top left: original Resolution Chart image. Top right: standard decompression. Bottom right: ICM without DC calibration. Bottom left: ICM with DC calibration. All images shown here are magnified by a factor of two.

the coefficients in a specified low-frequency zone are uniformly quantized, while the out-of-zone high-frequency coefficients are discarded [2]. Such a zonal sampling-based quantization scheme will be implemented in our experiments. Other quantization schemes can be found in [1] and [7].

C. Formulation of the MAP Estimation

The modified HMRF model based on (6) and the conditional probability given in (8), can be substituted in (2) for $p(x)$ and $p(y|x)$, respectively. The optimization is then derived as

$$\begin{aligned}\hat{X} &= \arg\min_{X\in\mathcal{X}} \sum_{c\in C} V_c(X) \\ &= \arg\min_{X\in\mathcal{X}} \sum_{m,n} \sum_{k,l\in c_{mn}} \rho(x_{mn} - x_{kl}) \end{aligned} \tag{9}$$

where c_{mn} is an 8-pixel neighborhood system of the current pixel at (m, n), and $\mathcal{X}$ is the constraint space

$$\mathcal{X} = \{X\colon y = \boldsymbol{Q}[\boldsymbol{H}(X)]\}. \tag{10}$$

The MAP estimation produces a smoothed update of the decompressed image. Such an estimation is then projected back to the constraint space $\mathcal{X}$. The projection is done in the transform domain in the following way:

$$\acute{y} = \begin{cases} d_i, & y < d_i \\ y, & d_i \le y < d_{i+1} \\ d_{i+1}, & y \ge d_{i+1} \end{cases} \tag{11}$$

in order to force the updated coefficient into the original quantization interval $[d_i, d_{i+1}]$. The projected image is then obtained by taking the inverse block DCT. Because the Huber function is convex, a convex constrained restoration problem is formed, and its convergence is guaranteed. To overcome the limitation of the basic MAP restoration in which the reference level errors of the whole block cannot be corrected, we propose to perform a DC calibration prior to the application of the MAP restoration. Moreover, both the DC calibration and the MAP restoration will be implemented using the ICM.

III. DC Calibration

The DC coefficients are of particular importance at low bit rates because they serve as the reference levels for all the pixels within each block, including the pixels along the block boundaries. Without prior DC calibration, subsequent processing such as the MAP restoration may result in further distortion beyond the original quantization errors, although the quantization errors may still be within the constrained ranges. As indicated by (11), the error range expands

to the *whole* quantization interval in the constrained restoration, as opposed to *half* of the interval during the original quantization. The uncertainty is doubled, since the projected coefficient may jump to the other half of the quantization interval level than where the original coefficient resides. This is more serious when the quantization intervals are often very large at low bit rates. Therefore, a smoothing technique cannot be expected to substantially improve the fidelity of the reconstruction in terms of PSNR, even though a visually pleasant image can be produced.

The primary constraint in the DC calibration comes from smoothness constraints on the transition of the image scene, namely, the gradient continuity. This is consistent with the HMRF image prior model, which implies the continuity of first derivatives. While the intensity continuity [8] imposes desired constraints in flat regions, gradient continuity constraint is a logical choice for both flat regions and slowly varying regions. We impose smoothness constraints on the gradient components perpendicular to the block boundary. The mean square difference between the gradient components and their estimates is minimized along the block boundaries subject to the constraints from the received data. As illustrated in Fig. 1, the gradient-continuity constraint avoids the possible overadjustment in a ramp region when the intensity-continuity constraint is enforced. The constrained DC estimation is given as

$$\hat{\boldsymbol{D}} = \arg \min_{\boldsymbol{D} \in \mathcal{D}} \sum_{B_{mn}} \sum_{s \in \partial B_{mn}} [g_s(\boldsymbol{D}) - \hat{g}_s]^2 \tag{12}$$

where $\boldsymbol{D}$ denotes the vector of all DC coefficients and $\mathcal{D}$ is the constraint space given by

$$\mathcal{D} = \{\boldsymbol{D}: \boldsymbol{Q}[\boldsymbol{D}] = \overline{\boldsymbol{D}} \text{ and } \overline{\boldsymbol{D}} \text{ is the quantized DC}\}. \tag{13}$$

g_s is the gradient at a boundary site s of the block B_{mn} and $\hat{g}_s$ is its estimation (see Fig. 1). Here, ∂B_{mn} denotes the set of all boundary points of the block B_{mn}.

To improve the efficiency of the DC calibration, we select a few anchor blocks to impose additional constraints. These anchor blocks serve as the controlling points and their DC coefficients are losslessly coded. In general, human attention tends to be in the center of the picture. For the same reason, the region-of-interest is, in many cases, in the center of various visual products such as painting, drawing, photo, film, and video. One natural layout of the anchor blocks reflecting human attention is illustrated in Fig. 2. It is true that the best choice of the anchor blocks would be scene-dependent. However, the criterion for such a choice is not clear without *a priori* knowledge of the image contents. A constraint on maintaining the same dynamic range is also enforced in the DC calibration. The particular layout of the anchor blocks facilitates a double spiral scan in the DC calibration, which starts from two central blocks to maximize the constraints between the current block and neighboring anchor blocks (or updated blocks). At the center of the image, the greater density of anchor blocks imposes stronger constraints, which decrease as the calibration spirals out. The anchor blocks also serve as resetting points to prevent error propagating. Note that the anchor blocks are located at the turning points of the spirals.

IV. Optimization Technique

The optimization technique is critical to the iterative solution of a constrained problem. A good optimization should be not only computationally efficient but also capable of converging to a desirable solution. An appropriate optimization technique should be carefully selected according to the nature of the problem. In this research, the *local* characteristics of an image are combined with the given compressed data to construct a MAP estimation of the original image. As discussed by Besag [11], certain large-scale characteristics of the model are often induced in choosing a nondegenerate field to describe the local properties of the scene. In general, the Markov random field may exhibit positive correlations over arbitrarily large distances in the iterative process so that adjacent pixels are very likely to be of same color or intensity. Therefore, in addition to computational efficiency, it is also a major concern to avoid such large-scale characteristics.

Some optimization techniques may lead to undesired computation or convergence difficulties. Simulated annealing [12], while it can guarantee the convergence to the global optimum, is computationally demanding and therefore impractical. Gradient descent [12] used in [9], is less computationally demanding, but it often converges to some local optimum of the objective function. Both methods are global optimization techniques, so that the reconstruction may suffer from some undesired large-scale properties of the random field due to the *simultaneous* optimization of the objective function.

ICM [11] is a computationally inexpensive local optimization technique, and is invulnerable to the large-scale characteristics. It was first proposed as an approximation to the Bayesian estimation that has overall maximum probability and later established itself as a distinctive optimization method that yields an estimation that has maximum probability at each individual pixel. A single cycle of the ICM only requires the *successive* minimization of the objective function at each pixel. Note that each pixel has only a few neighbors, and the dependence of the estimation on only the local characteristics is ensured by the rapid convergence of the ICM [11], typically within ten iterations. Therefore, the interference between pixels is limited and the undesired large-scale effects, such as oversmoothing, are minimized. With ICM implementations, we not only speed up the convergence, but, more important, we are able to obtain a better MAP estimation under the original assumption of a *localized* MRF.

V. Experiments and Discussions

We use 256×256 images in our experiments because images are often of relatively small sizes in low-bit-rate applications. Group 1 includes typical gray-scale images Lena, Peppers, USC Girl, and Boats to verify the reduction of the blocking artifact. Group 2 includes a document image "text" and a standard test image "resolution chart" to verify the reduction of the ringing artifact. Table I shows the bit rate and the corresponding PSNR for each test image. The proposed approach improves PSNR significantly in both groups. The PSNR improvements for Group 1 images range from 0.7 dB to over 1.0 dB, and those for Group 2 images range from 3.0 to 4.5 dB. PSNR improvement is especially valuable at low bit rates and often represents improved visual quality, as shown in Figs. 3–5. Note that the PSNR actually drops without DC calibration in the most challenging case of the Boats image (indicated by $*$ in Table I). The blocking artifact has been substantially reduced in all test images. The ringing effect is also effectively reduced, as demonstrated in Fig. 5. Notice that the image details are better preserved and the reconstructed images are much sharper if DC calibration is employed.

The additional coding cost of this approach comes from the coding of DC coefficients of the anchor blocks. Residues of these DC coefficients can be transmitted as a separate sparse image in which each block contains only the residue of corresponding DC coefficient followed directly by the EOB (end-of-block) sign. The increase in bit rate is insignificant (less than 2% in the experiments). Due to the ICM implementation, the computational complexity is comparable to many existing postprocessing methods.

VI. Conclusion

Three new aspects contribute to the overall success of the proposed approach. First, the DC calibration adjusts the reference level of a

TABLE I
PSNR EVALUATION OF THE RESULTS

image	bit rate (bpp)	DCT (dB)	DCC (dB)	ICM (dB)	DCCICM (dB)
lena	0.296	27.61	27.67	28.03	28.35
peppers	0.303	27.69	27.79	28.30	28.75
USC girl	0.197	30.03	30.39	30.94	31.25
boats	0.351	27.39	27.41	27.29*	27.77
text	0.435	16.59	17.11	18.19	19.48
chart	0.802	23.21	24.00	27.05	27.76

block *as a whole* and results in noticeable additional improvement in image quality, especially in terms of PSNR. Second, an improved HMRF model is developed to differentiate the artifacts from image details. Finally, the ICM implementation is not only computationally effective but also avoids undesired large-scale effects in enforcing the localized image model. In conclusion, the proposed scheme is able to improve the image quality both subjectively and objectively.

REFERENCES

[1] W. B. Pennebaker and J. L. Mitchell, *JPEG Still Image Data Compression Standard.* New York: Van Nostrand Reinhold, 1993.

[2] M. Rabbani and P. W. Jones, *Digital Image Compression Techniques.* Bellingham, WA: SPIE, 1991.

[3] H. C. Reeve and J. S. Lim, "Reduction of blocking effect in image coding," in *Proc. Int. Conf. Acoust., Speech, Signal Processing,* Boston, MA, 1983, pp. 1212–1215.

[4] H. S. Malvar and D. H. Staelin, "The LOT: transform coding without blocking effects," *IEEE Trans. Acoust., Speech, Signal Processing,* vol. 37, pp. 553–559, 1989.

[5] B. Ramamurthi and A. Gersho, "Nonlinear space-invariant post-processing of block coded images," *IEEE Trans. Acoust., Speech, Signal Processing,* vol. ASSP-34, pp. 553–559, 1986.

[6] K. Sauer, "Enhancement of low bit-rate coded images using edge detection and estimation," *CVGIP: Graphic. Models Image Processing,* vol. 53, pp. 52–62, 1991.

[7] R. Rosenholtz and A. Zakhor, "Iterative procedures for reduction of blocking effects in transform image coding," *IEEE Trans. Circuits Syst. Video Technol.,* vol. 2, pp. 91–94, Mar. 1992.

[8] Y. Yang, N. P. Galatsanos, and A. K. Katsaggelos, "Regularized reconstruction to reduce blocking artifacts of block discrete cosine transform compressed images," *IEEE Trans. Circuits Syst. Video Technol.,* vol. 3, pp. 421–432, Dec. 1993.

[9] R. L. Stevenson, "Reduction of coding artifacts in transform image coding," in *Proc. Int. Conf. Acoust., Speech, Signal Processing,* Minneapolis, MN, 1993, pp. V401–404.

[10] Z. Fan and R. Eschbach, "JPEG decompression with reduced artifacts," in *Proc. IS&T/SPIE Symp. Electron. Imaging: Image Video Compress.,* San Jose, CA, Feb. 1994.

[11] J. Besag, "On the statistical analysis of dirty pictures," *J. Royal Stat. Soc.,* vol. 48, pp. 259–302, 1986.

[12] S. Geman and D. Geman, "Stochastic relaxation, Gibbs distribution, and the Bayesian restoration of images," *IEEE Trans. Pattern Anal. Machine Intell.,* vol. PAMI-6, pp. 721–741, 1984.

Differential Block Coding of Bilevel Images

George R. Robertson, Maurice F. Aburdene, and Richard J. Kozick

Abstract— **In this correspondence, a simple one-dimensional (1-D) differencing operation is applied to bilevel images prior to block coding to produce a sparse binary image that can be encoded efficiently using any of a number of well-known techniques. The difference image can be encoded more efficiently than the original bilevel image whenever the average run length of black pixels in the original image is greater than two. Compression is achieved because the correlation between adjacent pixels is reduced compared with the original image. The encoding/decoding operations are described and compression performance is presented for a set of standard bilevel images.**

I. INTRODUCTION

The storage and/or transmission requirements of binary images are proportional to the number of pixels in the image. Two methods for reducing these requirements are lossless [1]–[5] and lossy [6] compression. Kunt and Johnsen [3], [7], [8] investigated block coding methods for image compression. Block coding takes advantage of the small number of black pixels relative to the number of white pixels by breaking the image into blocks and only coding the blocks that contain black pixels. Zeng and Ahmed [1] and Kavalerchik [2] have shown that bilevel images composed of sparse binary patterns can be efficiently compressed with block coding. Zeng and Ahmed's (ZA) block coding scheme assumes random binary patterns and achieves compression if the density of black pixels is less than 19%.

References [1], [2] indicate that text documents are not well-modeled as sparse, random, binary patterns, but after some decorrelation or prediction procedures, they can be well-approximated as random, binary patterns. This paper presents a very simple decorrelation method for one-dimensional (1-D) blocks by performing differences between adjacent pixel values that can be implemented by an EXCLUSIVE-OR gate. General block coding methods can be applied to the difference image, such as those of Kunt and Johnsen

Manuscript received September 20, 1994; revised January 22, 1996. The associate editor coordinating the review of this manuscript and approving it for publication was Dr. Amy R. Reibman.

G. R. Robertson is with Harris RF Communications, Rochester, NY 14610 USA.

M. F. Aburdene and R. J. Kozick are with the Department of Electrical Engineering, Bucknell University, Lewisburg, PA 17837 USA (e-mail: aburdene@bucknell.edu).

Publisher Item Identifier S 1057-7149(96)05266-9.